Cell Stress and Chaperones (2010) 15:309–322
DOI 10.1007/s12192-009-0145-6

ORIGINAL PAPER

The topical antimicrobial zinc pyrithione is a heat shock response inducer that causes DNA damage and PARP-dependent energy crisis in human skin cells

Sarah D. Lamore · Christopher M. Cabello · Georg T. Wondrak

Received: 1 July 2009 / Revised: 2 September 2009 / Accepted: 14 September 2009 / Published online: 7 October 2009

Abstract The differentiated epidermis of human skin serves as an essential barrier against environmental insults from physical, chemical, and biological sources. Zinc pyrithione (ZnPT) is an FDA-approved microbicidal agent used worldwide in clinical antiseptic products, over-the-counter topical antimicrobials, and cosmetic consumer products including antidandruff shampoos. Here we demonstrate for the first time that cultured primary human skin keratinocytes and melanocytes display an exquisite vulnerability to nanomolar concentrations of ZnPT resulting in pronounced induction of heat shock response gene expression and impaired genomic integrity. In keratinocytes treated with nanomolar concentrations of ZnPT, expression array analysis revealed massive upregulation of genes encoding heat shock proteins (*HSPA6*, *HSPA1A*, *HSPB5*, *HMOX1*, *HSPA1L*, and *DNAJA1*) further confirmed by immunodetection. Moreover, ZnPT treatment induced rapid depletion of cellular ATP levels and formation of poly (ADP-ribose) polymers. Consistent with an involvement of poly(ADP-ribose) polymerase (PARP) in ZnPT-induced energy crisis, ATP depletion could be antagonized by pharmacological inhibition of PARP. This result was independently confirmed using PARP-1 knockout mouse embryonic fibroblasts that were resistant to ATP depletion and cytotoxicity resulting from ZnPT exposure. In keratinocytes and melanocytes, single-cell gel electrophoresis and flow cytometric detection of γ-H2A.X revealed rapid induction of DNA damage in response to ZnPT detectable before general loss of cell viability occurred through caspase-independent pathways. Combined with earlier experimental evidence that documents penetration of ZnPT through mammalian skin, our findings raise the possibility that this topical antimicrobial may target and compromise keratinocytes and melanocytes in intact human skin.

Keywords Zinc pyrithione · Keratinocyte · Melanocyte · Comet assay · Heat shock response · PARP-dependent ATP depletion

Abbreviations

3-ABA	3-Aminobenzamide
AV	AnnexinV
FITC	Fluorescein isothiocyanate
DTPA	Diethylenetriaminepentaacetic acid
EGR1	Early growth response protein 1
Fpg	Formamidopyrimidine-glycosylase
HEK	Human epidermal keratinocyte
HEM	Human epidermal melanocyte
HO-1	Heme oxygenase 1
HSP	Heat shock protein
MEF	Mouse embryonal fibroblast
NAC	*N*-Acetyl-L-cysteine
OTC	Over-the-counter
PAR	Poly(ADP-ribose) polymer
PARP	Poly(ADP-ribose) polymerase
PI	Propidium iodide
SDS-PAGE	Sodium dodecylsulfate polyacrylamide gel electrophoresis
ZnPT	Zinc pyrithione

S. D. Lamore · C. M. Cabello · G. T. Wondrak
Department of Pharmacology and Toxicology,
College of Pharmacy, Arizona Cancer Center,
University of Arizona,
Tucson, AZ, USA

G. T. Wondrak (✉)
College of Pharmacy & Arizona Cancer Center,
University of Arizona,
1515 North Campbell Avenue,
Tucson, AZ 85724, USA
e-mail: wondrak@pharmacy.arizona.edu

Introduction

The differentiated epidermis of human skin serves as an essential barrier against environmental insults from physical (e.g., solar ultraviolet radiation), chemical (e.g., xenobiotics), and microbial sources (Chuong et al. 2002; Wondrak 2007a). Epidermal cells, including keratinocytes, melanocytes, and antigen-presenting Langerhans cells, are key targets of environmental stressors leading to accumulative damage and functional alterations thought to play major roles in skin dysfunction and carcinogenesis (Baudouin et al. 2002; Wondrak 2007a).

Much research has focused on the identification and development of drug-like molecules for the prevention of skin damage from environmental insult, particularly photodamage from solar UV radiation (Halliday 2005; Kullavanijaya and Lim 2005; Wondrak et al. 2006; Wondrak 2007a; Jonak et al. 2009). Research from various groups, including our own, has shown that small molecule inducers of the heat shock and Nrf2 (nuclear factor-E2-related factor 2) oxidative stress response pathways exert chemopreventive activity with suppression of skin cell photodamage, photooxidative stress, and photocarcinogenesis (Dinkova-Kostova et al. 2006; Merwald et al. 2006; Wondrak et al. 2008).

Zinc is an important micronutrient and prototype inducer of cytoprotective mechanisms including signaling through Nrf2 and upregulation of metallothionein and heat shock protein expression, all of which have been observed upon exposure to inorganic zinc salts (e.g., $ZnSO_4$) in the submillimolar (100–200 μM) concentration range (Hatayama et al. 1993; Jourdan et al. 2002; Cortese et al. 2008). In an attempt to explore the potential cytoprotective activity of topical Zn compounds for skin protection against environmental insults, we focused our research efforts on zinc pyrithione (ZnPT; CAS number: 13463-41-7), a 1:2 complex between a central zinc atom and the membrane permeable ionophore pyrithione (*N*-hydroxy-2-pyridinethione; Barnett et al. 1977).

ZnPT is an FDA-approved microbicidal agent used worldwide in clinical antiseptic products, over-the-counter (OTC) topical antimicrobials, and cosmetic consumer products, including antidandruff shampoos, where typical ZnPT concentrations are in the range of 1% to 2% (*w*/*v*; Pierard-Franchimont et al. 2002; Bailey et al. 2003; Guthery et al. 2005). Epidermal deposition and retention of the lipophilic metal chelate ZnPT following topical application has been demonstrated in human skin (Rutherford and Black 1969; Leyden et al. 1979), and percutaneous penetration of ZnPT through rat, rabbit, guinea pig, and rhesus monkey skin has been documented earlier (Okamoto et al. 1967; Howes and Black 1975; Gibson and Calvin 1978; Guthery et al. 2005). Topical safety and toxicity profile of this OTC-drug have been studied to some extent previously, and it has been established that ZnPT does not display a potential for primary irritation or sensitization of human skin (Snyder et al. 1965; Brandrup and Menne 1985; Skoulis et al. 1993).

Paradoxically, no studies have examined ZnPT cyto- and genotoxicity in human skin cells as the likely target cells of topically administered ZnPT. Moreover, no valid studies with ZnPT are available to satisfy the data requirements for carcinogenicity assessment of this chemical as stated recently in the *AD Risk Assessment for the Reregistration Eligibility Decision (RED) Document on ZnPT* prepared by the US Environmental Protection Agency (Smegal et al. 2004).

Our initial experiments did not substantiate a potential cytoprotective activity of ZnPT, but suggested that exposure of cultured human skin cells to this topical drug is associated with cytotoxic adverse effects observed after short exposure to submicromolar concentrations. Here we demonstrate for the first time that primary human skin keratinocytes and melanocytes display an exquisite vulnerability to ZnPT resulting in pronounced induction of heat shock response gene expression and rapid loss of genomic integrity with PARP-1-dependent ATP depletion.

Materials and methods

Materials All chemicals, including ZnPT (CAS number: 13463-41-7), were from Sigma Chemical Co. (St. Louis, MO, USA). A 1 mM stock solution of ZnPT was prepared by dissolving the compound in DMSO. The cell-permeable pan-caspase inhibitor Z-VAD-(OMe)-fmk was purchased from Calbiochem-Novabiochem (San Diego, CA, USA). The poly(ADP-ribose) polymerase (PARP) inhibitors 3-aminobenzamide and PJ-34 were from Sigma and Enzo Life Sciences Inc. (Farmingdale, NY, USA), respectively.

General cell culture Primary human epidermal keratinocytes (neonatal HEKn-APF, from Cascade Biologics, Portland, OR, USA) were cultured using Epilife medium supplemented with EDGS growth supplement. Primary human melanocytes (HEMa-LP, from Cascade Biologics) were cultured using Medium 154 medium supplemented with HMGS2 growth supplement. Both cell lines were passaged using recombinant trypsin/EDTA and defined trypsin inhibitor. Cells were maintained at 37°C in 5% CO_2, 95% air in a humidified incubator.

PARP-1$^{-/-}$ mouse embryonic fibroblasts Mouse embryonic fibroblasts (MEFs) derived from both PARP-1 wild-type

(PARP-$1^{+/+}$) and PARP-$1^{-/-}$ mice generated by Z. Q. Wang (Institute of Molecular Pathology, Vienna; Wang et al. 1995) were kindly provided by M.K. Jacobson, College of Pharmacy & Arizona Cancer Center, University of Arizona. MEFs were cultured at 37°C (5% CO_2) in DMEM supplemented with 10% BCS.

Cell proliferation assay Cells were seeded at 10,000 cells/dish on 35-mm dishes. After 24 h, cells were treated with test compound. Cell number at the time of compound addition and 72 h later were determined using a Z2 Analyzer (Beckman Coulter, Inc., Fullerton, CA, USA) as described recently (Wondrak et al. 2003). Proliferation was compared with cells that received mock treatment. The same methodology was used to establish IC_{50} values (drug concentration that induces 50% inhibition of proliferation of treated cells within 72 h of exposure ± SD, $n=3$).

Cell death analysis Viability and induction of cell death (early and late apoptosis/necrosis) were examined by annexinV-FITC/propidium iodide (PI) dual staining of cells followed by flow cytometric analysis using an apoptosis detection kit according to the manufacturer's specifications (APO-AF, Sigma) as published previously (Wondrak 2007b).

Caspase-3 activation assay Treatment-induced caspase-3 activation was examined in human epidermal keratinocytes (HEKs) using a cleaved/activated caspase-3 (asp 175) antibody (Alexa Fluor 488 conjugate, Cell Signaling, Inc., Danvers, USA) followed by flow cytometric analysis as published recently (Wondrak 2007b).

Cellular ATP assay Cells were seeded at 5,000 cells/well of an opaque 96-well plate. After 24 h, cells were treated with test compound. At various time points, ATP content per well was determined using the CellTiter-Glo luminescent assay (Promega, Madison, WI, USA) according to the manufacturer's instructions. Data are normalized to ATP content in untreated cells and expressed as means ± SD ($n=3$).

Detection of intracellular oxidative stress by flow cytometric analysis ZnPT-induced generation of intracellular oxidative stress was analyzed by flow cytometry using 2′,7′-dichlorodihydrofluorescein diacetate (DCFH-DA) as a sensitive nonfluorescent precursor dye according to a published standard procedure (Cabello et al. 2009a). In brief, ZnPT-treated and untreated control cells on dishes were washed with PBS and incubated for 60 min in the dark (37°C, 5% CO_2) with culture medium containing DCFH-DA (5 μg/mL final concentration). Cells were then washed with PBS, harvested by trypsinization, resuspended in 300 μL PBS, and immediately analyzed by flow cytometry.

Determination of total cellular glutathione content Pharmacological modulation of intracellular glutathione content was analyzed using the photometric HT Glutathione Assay Kit (Trevigen, Gaithersburg, MD, USA) based on the enzymatic recycling method involving glutathione reductase and DTNB (5,5′-dithiobis-2-nitrobenzoic acid, Ellman's reagent). HEKs (1×10^6) were exposed to a dose range of ZnPT (6 h of exposure time) and harvested by trypsinization followed by sample processing according to the manufacturer's instructions. Glutathione content of total cellular extracts was normalized to protein content determined using the BCA assay (Pierce, Rockford, IL, USA).

Comet assay (alkaline single cell gel electrophoresis) The alkaline Comet assay was performed according to the manufacturer's instructions (Trevigen, Gaithersburg, MD, USA) as published recently (Wondrak et al. 2003; Cabello et al. 2009b). Cells were seeded at 100,000 per 35-mm dish 24 h prior to treatment. Untreated cells were used as a negative control group. After treatment, cells were harvested by gently scraping, rinsed with ice-cold DPBS, and suspended in 500 μL DPBS. The cell suspension (50 μL) was mixed with 450 μL low-melting-point agarose and spread on pretreated microscope slides. Slides were allowed to dry protected from light, then immersed in ice-cold lysis solution plus 10% DMSO and incubated at 4°C for 45 min. To allow DNA unwinding and expression of alkali-labile sites, slides were exposed to alkaline buffer (1 mmol/L EDTA and 300 mmol/L NaOH, pH>13) protected from light at room temperature for 45 min. Electrophoresis was conducted in the same alkaline buffer for 20 min at 300 mA. After electrophoresis, slides were rinsed three times in ddH2O then fixed in 70% ethanol for 5 min. Slides were dried for at least 1 h at 32°C. Cells were then stained with SYBR® Green and analyzed with a fluorescence microscope (fluorescein filter) and analyzed using CASP software. At least 100 tail moments for each group were analyzed in order to calculate the mean ± SD for each group. The formamidopyrimidine-glycosylase (Fpg) FLARE assay for assessment of Fpg-induced strand cleavage at oxidized purine bases was performed according to the manufacturer's instructions (Trevigen). In brief, comet analysis was performed as described above, except that after lysis slides were washed with FLARE buffer three times and then incubated with Fpg enzyme solution (2 U Fpg/75 μL buffer/slide) or buffer only for 30 min at 37°C.

Phospho-H2A.X detection by flow cytometry Treatment-induced accumulation of nuclear phosphorylated histone variant H2A.X (γ-H2A.X) was examined in HEKs as published recently using a phospho-histone H2A.X (Ser139) monoclonal antibody (Alexa Fluor 488 conjugate, Cell Signaling, Inc., Danvers, MA, USA) followed by flow cytometric analysis (Cabello et al. 2009b).

Human Stress and Toxicity PathwayFinder™ RT² Profiler™ PCR Expression Array After pharmacological exposure, total cellular RNA (5×10^6 NHEKs) was prepared using the RNeasy kit (Qiagen, Valencia, CA, USA) according to the manufacturer's instructions. Reverse transcription was performed using the RT² First Strand kit (SA Biosciences, Frederick, MD, USA) and 1 μg total RNA. The Human Stress and Toxicity PathwayFinder™ RT² Profiler™ PCR Expression Array (SuperArray, Frederick, MD, USA) profiling the expression of 84 stress- and toxicity-related genes was run as published recently (Cabello et al. 2009a), using the following PCR conditions: 95°C for 10 min, followed by 40 cycles of 95°C for 15 s alternating with 60°C for 1 min (Applied Biosystems 7000 SDS, Foster City, CA, USA). Gene-specific product was normalized to GAPDH and quantified using the comparative ($\Delta\Delta C_t$) Ct method as described in the ABI Prism 7000 sequence detection system user guide. Expression values were averaged across three independent array experiments, and standard deviation was calculated for graphing.

PARP immunoblot analysis Cells (1×10^6) were lysed using 1× SDS-PAGE sample buffer (0.375 M Tris HCl pH 6.8, 50% glycerol, 10% SDS, 5% β-mercaptoethanol, 0.25% bromophenol blue). After SDS-PAGE (4–12% gradient gel, Bio-Rad, Hercules, CA, USA), semidry transfer onto a nitrocellulose membrane (Optitran, Whatman, Bedford, MA, USA) was performed, followed by incubation in blocking buffer [TBST (0.1% Tween 20), 5% nonfat dry milk] for 1 h at 25°C. Membranes were washed three times with TBST and incubated overnight at 4°C with a monoclonal rabbit anti-PARP antibody diluted 1:1,000 (46D11, Cell Signaling) in incubation buffer (TBST, 5% BSA). Incubation with HRP-conjugated goat antirabbit antibody (Jackson Immunoresearch Laboratories, West Grove, PA, USA) at 1:20,000 dilution was then followed by visualization using enhanced chemiluminescence reagents.

Poly(ADP-ribose) immunoblot analysis One day before treatment, 1×10^6 cells were seeded in a 100-mm² dish. After 24 h, cells were treated with test compound. After treatment, cells were washed with PBS, lysed in 1× SDS-PAGE sample buffer, and heated for 3 min at 95°C prior to separation by 4–12% SDS-PAGE (Bio-Rad). After separation, proteins were transferred electrophoretically to a nitrocellulose membrane. Equal protein loading was examined by Ponceau S stain (0.1% in 1% acetic acid). After blocking in 5% milk-TBST, mouse anti-poly(ADP-ribose) polymer (PAR) monoclonal antibody (Trevigen) was used 1:1,000 in 5% milk-TBST overnight at 4°C. Incubation with HRP-conjugated goat antimouse antibody (Jackson Immunoresearch Laboratories) at 1:20,000 dilution was then followed by visualization using enhanced chemiluminescence reagents.

Heme oxygenase-1 immunoblot analysis One day before treatment, 1×10^6 cells were seeded in a T-75 flask. After 24 h, cells were treated with test compound. After exposure (37°C, 5% CO_2), cells were washed with PBS, lysed in 1× SDS-PAGE sample buffer, and heated for 3 min at 95°C prior to separation by 12% SDS-PAGE. Rabbit antiheme oxygenase-1 (HO-1) polyclonal antibody (Assay Designs, Inc., Ann Arbor, MI, USA) was used 1:5,000 in 5% milk-PBST overnight at 4°C. Incubation with HRP-conjugated goat antirabbit antibody (Jackson Immunoresearch Laboratories) at 1:20,000 dilution was then followed by visualization using enhanced chemiluminescence reagents. Equal protein loading was examined by α-actin-detection using a mouse antiactin monoclonal antibody (Sigma).

HSP70 immunoblot analysis Cell extraction, 12% SDS-PAGE, and Western transfer were performed as specified for HO-1 immunoblot analysis. Rabbit anti-HSP70 polyclonal antibody (SPA-811; Assay Designs) was used 1:1,500 in 5% milk-PBST overnight at 4°C. The membrane was processed for visualization using enhanced chemiluminescence as described for HO-1 immunodetection.

HSPA6 ELISA The enzyme-linked immunosorbent assay for HSPA6 (also called Hsp70B′) was performed in 96 well format on cell lysates extracted from treated cells following kit instructions ("Hsp70B prime" ELISA Kit; Assay Designs). Briefly, 1×10^6 cells were seeded per T-75 flask 1 day before treatment. Cells (3×10^6 per group) were exposed to test compound for 24 h (37°C, 5% CO_2) and then harvested, washed with PBS, and lysed in 1× extraction reagent. After protein quantification using the BCA assay, samples were diluted to a range within the Hsp70B′ standard curve and processed according to the manufacturer's instructions. Absorbance (450 nm) was determined on a microtiter plate reader (Versamax, Molecular Devices, Sunnyvale, CA, USA). Data represent the average of three independent experiments.

Statistical analysis Unless indicated differently, the results are presented as means ± SD of at least three independent

experiments. They were analyzed using the two-sided Student's *t* test (*$p<0.05$; **$p<0.01$; ***$p<0.001$).

Results

ZnPT induces a massive heat shock response in human epidermal keratinocytes First, modulation of stress response gene expression was examined in cultured human epidermal keratinocytes (HEKs) exposed to submicromolar concentrations of ZnPT using the RT^2 Human Stress and Toxicity Pathway Finder™ PCR Expression Array technology that allows simultaneous assessment of heat shock and antioxidant response gene expression (Cabello et al. 2009a; Cabello et al. 2009b). ZnPT treatment (500 nM, 24 h) altered expression levels of ten genes on the array by at least 3-fold (Fig. 1), including genes encoding the heat shock proteins HSPA6 (*HSPA6*; 129-fold), HSPA1A (*HSPA1A*; 35-fold), HSPA1L (*HSPA1L*; 7-fold), HSPB5 (*HSPB5*; 29-fold), and DNAJA1 (*DNAJA1*; 3-fold), the heat shock protein and antioxidant enzyme hemeoxygenase-1 (*HMOX1*; 7-fold), and the stress-responsive transcription factor early growth response protein 1 (*EGR1*; 6-fold).

Next, ZnPT-induced upregulation of major target genes, including *HSPA6*, *HSPA1A*, and *HMOX1*, was confirmed at the protein level (Fig. 2). Indeed, HSPA6 (also called Hsp70B′), a protein not constitutively expressed and induced only under conditions of extreme cellular stress, was upregulated more than 250-fold in response to ZnPT (500 nM, 24 h) as assessed by ELISA analysis (Fig. 2a; Noonan et al. 2007). Consistent with the results obtained by HSPA6 analysis, pronounced upregulation of HSP70 was observed in HEKs exposed to ZnPT (Fig. 2b, c), but not in cells exposed to $ZnSO_4$ (1 μM; data not shown). Cellular HSP70 levels were upregulated within 3 h of exposure, and maximal levels were observable at 6 h. Similarly, pronounced upregulation of cellular levels of HO-1, the protein encoded by *HMOX1*, was observed after 3 h of exposure to ZnPT (Fig. 2b, c).

Taken together, these findings indicate that nanomolar concentrations of ZnPT induce a rapid stress response in HEKs characterized by massive heat shock response gene expression that is associated with upregulation of HSP70, HSPA6, and HO-1 protein levels.

ZnPT inhibits proliferation and induces caspase-independent cell death in human epidermal keratinocytes Next, modulation of HEK proliferation and viability by exposure to ZnPT were assessed. Significant inhibition of cell proliferation was observed at low nanomolar concentrations of ZnPT (IC_{50} 256.8±14.4 nM; Fig. 3a). In contrast, no inhibition of proliferation was observed in response to $ZnSO_4$ exposure examined at similar concentrations. At higher concentrations of ZnPT (≥500 nM) morphological changes consistent with induction of cell death, including cell rounding and detachment, were observed within 24 h of exposure. We therefore examined the ability of ZnPT to induce cell death in HEKs using flow cytometric analysis of annexinV/propidium iodide (AV/PI) stained cells (Fig. 3b–

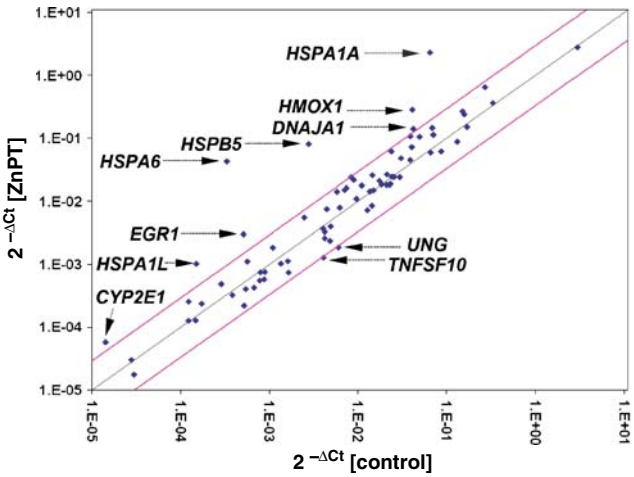

gene symbol	fold change	p-value
HSPA6 (NM_002155)	129.0	0.006
HSPA1A (NM_00534)	35.2	0.001
HSPB5 (NM_001885)	28.8	0.006
HMOX1 (NM_002133)	6.9	0.010
HSPA1L (NM_005527)	6.8	0.012
EGR1 (NM_001964)	5.9	0.007
CYP2E1 (NM_000773)	4.1	0.010
DNAJA1 (NM_001539)	3.3	0.015
TNFSF10 (NM_003810)	-3.2	0.002
UNG (NM_003362)	-3.2	0.023

Fig. 1 Gene expression array analysis of ZnPT-treated human skin keratinocytes. Differential gene expression in HEKs exposed to ZnPT (500 nM; 24 h) or left untreated was analyzed using the RT^2 Human Stress and Toxicity Pathway Finder™ PCR Expression Array performed in three independent repeat experiments and analyzed using the two-sided Student's *t* test. Changes in cycle threshold (*Ct*) for genes of interest relative to GAPDH for untreated control (*x*-axis) versus ZnPT-treated (*y*-axis) cells are displayed as scatter blot. *Upper and lower lines* represent the cutoff indicating 3-fold up- or downregulated expression, respectively. The *arrows* specify the ten genes with statistically significant ($p<0.05$) ZnPT-induced up- or downregulation of expression by at least 3-fold as summarized in the *table*

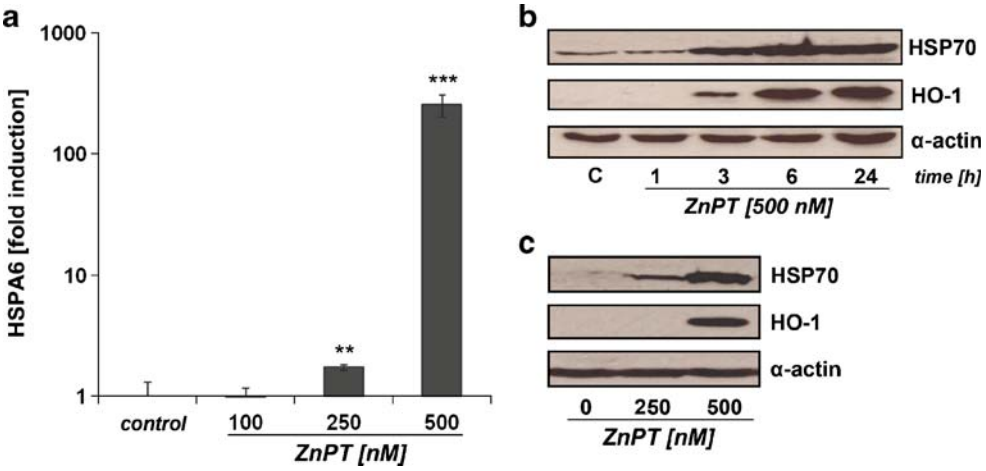

Fig. 2 Upregulation of HSPA6, HSP70, and HO-1 protein levels in ZnPT-treated human skin keratinocytes. **a** Induction of HSPA6 protein expression in ZnPT-treated HEKs was determined by ELISA analysis at 24-h exposure. **b** and **c** Western blot analysis of ZnPT-induced HSP70 and HO-1 upregulation was performed in HEKs. **b** Time course of HSP70 and HO-1 upregulation induced by ZnPT. **c** Dose response of ZnPT-induced HSP70 and HO-1 upregulation analyzed at 24-h exposure

d). A detailed dose response (100 to 1,000 nM ZnPT, 24 h) analysis indicated that induction of cell death required a threshold concentration of approximately 500 nM, and no viable cells were detected after 24 h of exposure to concentrations as low as 1,000 nM (Fig. 3b). Time course analysis showed that cell viability (AV^-/PI^-) was maintained for at least 6 h of continuous exposure (500 nM ZnPT; Fig. 3c). Interestingly, at all time points and concentrations, cells with impaired viability stained mostly double positive (AV^+/PI^+), indicative of cells in late apoptosis and/or necrosis, and only a few cells were located in the lower right quadrant (AV^+/PI^-) indicative of early apoptosis (Fig. 3b–d). Consistent with a caspase-independent mechanism of cell death, ZnPT-induced loss of cell viability was not influenced by the presence of the pan-caspase inhibitor zVAD-fmk (Fig. 3d), and no proteolytic activation of caspase 3 occurred in response to ZnPT exposure as demonstrated by flow cytometric analysis using an Alexa 488-conjugated antibody that recognizes cleaved procaspase 3 (data not shown). Consistent with earlier findings that demonstrate zinc-dependent induction of mammalian cell death in response to ZnPT exposure (Kim et al. 1999; Mann and Fraker 2005; Klein et al. 2006; Magda et al. 2008), cotreatment with the cell impermeable zinc chelator diethylenetriaminepentaacetic acid (DTPA) completely protected from ZnPT-induced cell death (Fig. 3d). Interestingly, complete suppression of ZnPT cytotoxicity was also observed when exposure occurred in the presence of the thiol antioxidant *N*-acetyl-L-cysteine (NAC, Fig. 3d). However, other antioxidant agents, including superoxide dismutase (SOD), catalase, L-ascorbic acid, and the cell-permeable SOD^- and catalase-mimetic EUK-114 did not antagonize ZnPT cytotoxicity in HEKs (data not shown).

Taken together, these data suggest that ZnPT inhibits proliferation of HEKs at nanomolar concentrations and that loss of HEK viability observed at ZnPT concentrations equal to or higher than 500 nM involves a caspase-independent mechanism of cell death.

ZnPT treatment induces rapid depletion of cellular ATP that is antagonized by pharmacological and genetic inhibition of PARP In an attempt to identify functional alterations that precede ZnPT-induced loss of HEK viability, we examined changes in cellular energy status by monitoring ATP levels during exposure to ZnPT. Significant depletion of cellular ATP levels was detectable in HEKs within 1 h of exposure to ZnPT and exceeded 50% after 6 h (Fig. 4a). In contrast, no depletion of ATP levels was observed with $ZnSO_4$ (1 μM; data not shown), and cotreatment with DTPA reduced ZnPT-induced depletion of ATP (Fig. 4b), consistent with antagonism of ZnPT-induced cytotoxicity by this potent Zn-ion chelator as observed in Fig. 3d. Importantly, these early changes in ATP levels occurred without loss of viability and impaired membrane integrity as verified by AV/PI analysis (Fig. 3c) and confirmed independently using the trypan blue exclusion assay (data not shown).

Fig. 3 Antiproliferative and cell death-inducing activity of ZnPT in human skin keratinocytes. **a** Dose response relationship of ZnPT-induced inhibition of cell proliferation. After 72 h of exposure to increasing concentrations of ZnPT and $ZnSO_4$ (1 μM), proliferation was examined by cell counting and expressed as % of untreated control (mean ± SD, $n \geq 3$). Representative light microscopy pictures were taken after 72 h of exposure; *I* control, *II* ZnPT (250 nM), *III* ZnPT (400 nM). **b** Dose response of ZnPT-induced cell death. Cells were exposed to ZnPT (24 h) or left untreated, and viability was assessed by flow cytometric analysis of AV-FITC/PI-stained cells. **c** Time course of ZnPT-induced cell death. Cells were exposed to ZnPT or left untreated, and viability was assessed by flow cytometric analysis. **d** Induction of cell death upon extended exposure (24 h) to ZnPT in the absence or presence of the pan-caspase inhibitor zVADfmk (42 μM), NAC (10 mM), or DTPA (60 μM) was assessed by flow cytometric analysis. The *numbers* indicate viable cells (AV^-, PI^-, *lower left quadrant*) in percent of total gated cells (mean ± SD, three independent experiments). Flow cytometric panels depict one representative experiment

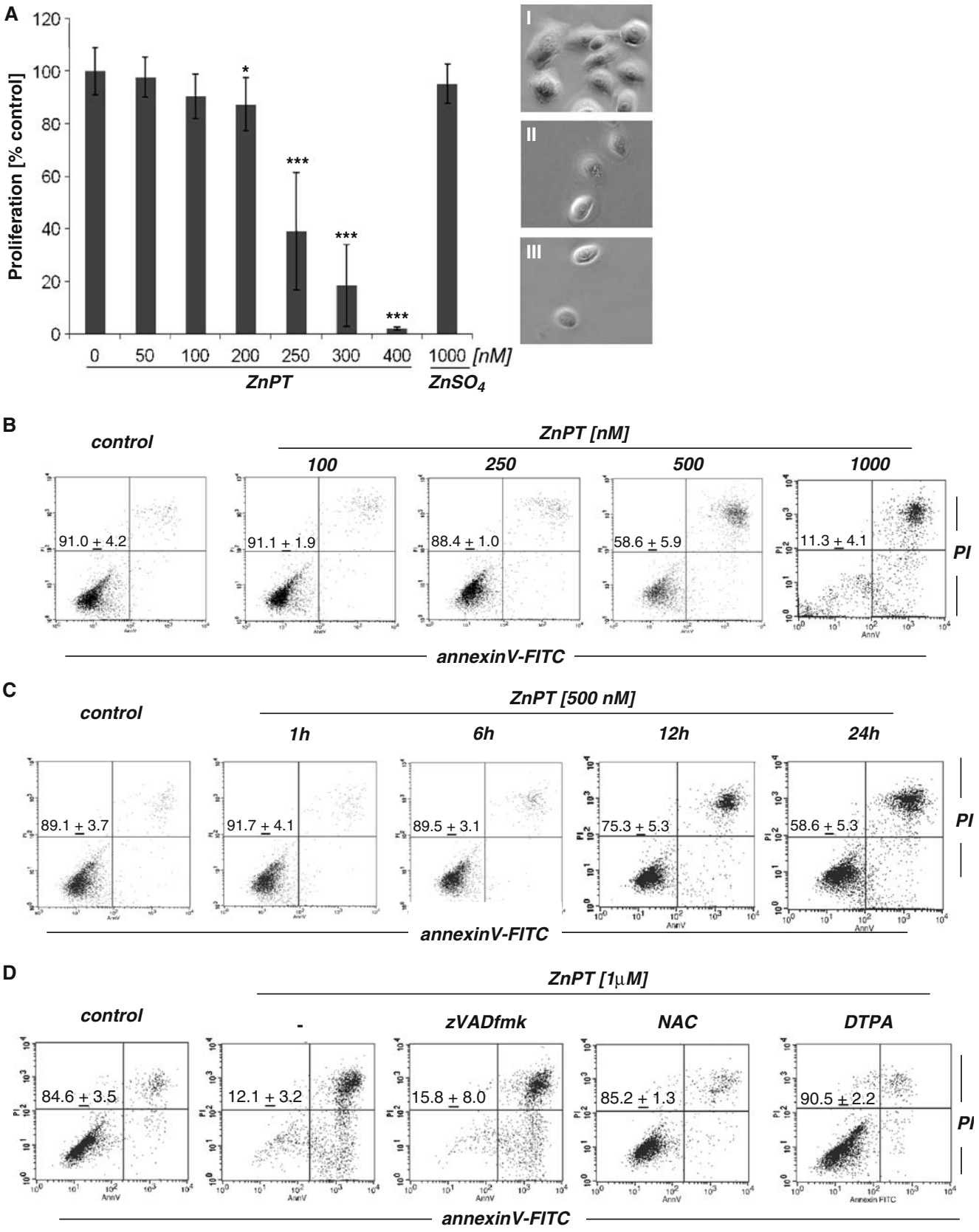
A
Proliferation [% control]
120
100
80
60
40
20
0
*
***
***
***
0
50
100
200
250
300
400
1000 [nM]
ZnPT
ZnSO4
I
II
III
B
control
ZnPT [nM]
100
250
500
1000
91.0 ± 4.2
91.1 ± 1.9
88.4 ± 1.0
58.6 ± 5.9
11.3 ± 4.1
PI
annexinV-FITC
C
control
ZnPT [500 nM]
1h
6h
12h
24h
89.1 ± 3.7
91.7 ± 4.1
89.5 ± 3.1
75.3 ± 5.3
58.6 ± 5.3
PI
annexinV-FITC
D
control
ZnPT [1μM]
-
zVADfmk
NAC
DTPA
84.6 ± 3.5
12.1 ± 3.2
15.8 ± 8.0
85.2 ± 1.3
90.5 ± 2.2
PI
annexinV-FITC

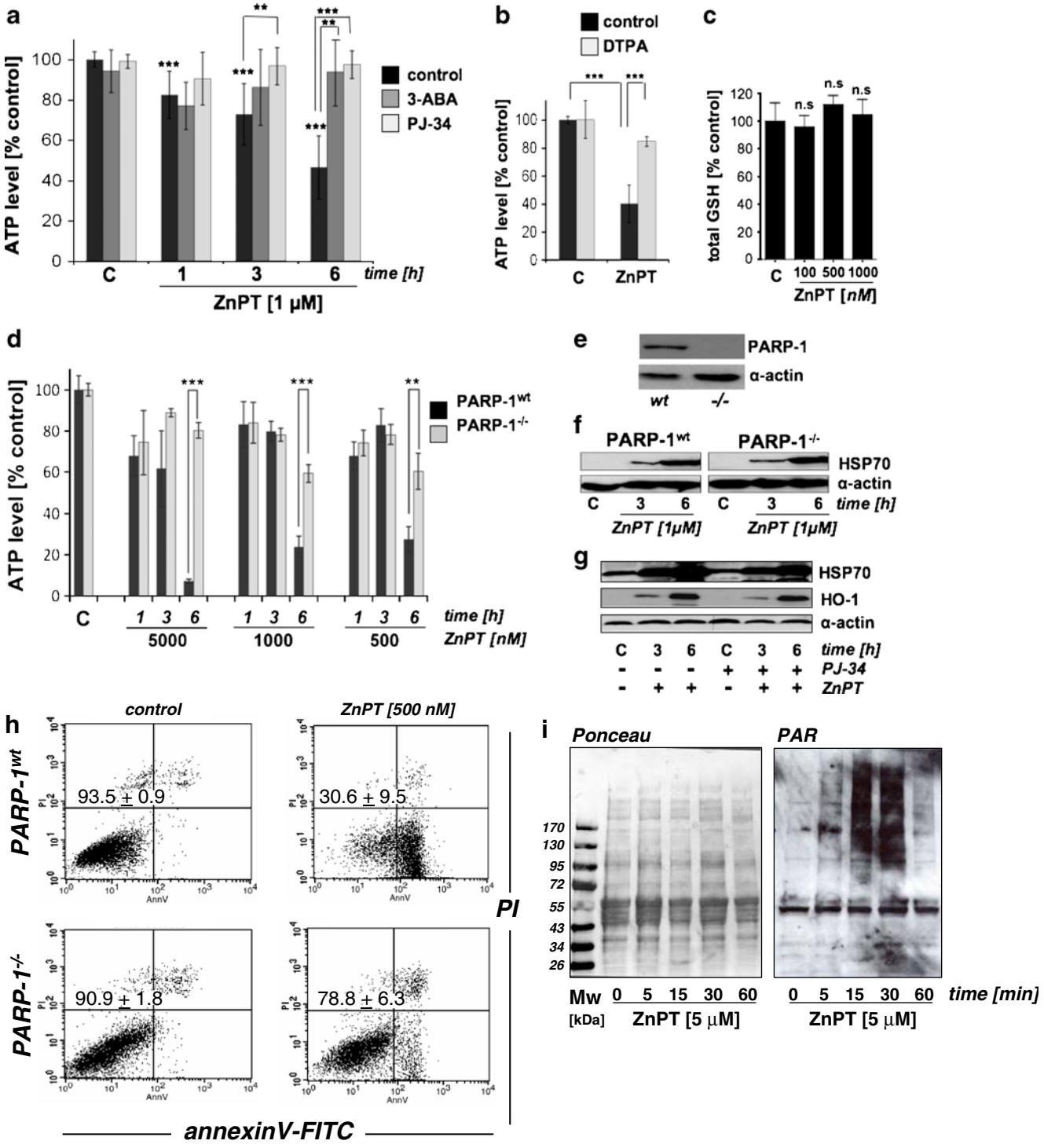
a
ATP level [% control]
control
3-ABA
PJ-34
C
1
3
6
time [h]
ZnPT [1 μM]
b
control
DTPA
ATP level [% control]
C
ZnPT
c
total GSH [% control]
n.s
C
100 500 1000
ZnPT [nM]
d
ATP level [% control]
PARP-1wt
PARP-1-/-
time [h]
ZnPT [nM]
5000
1000
500
e
PARP-1
α-actin
wt
-/-
f
PARP-1wt
PARP-1-/-
HSP70
α-actin
time [h]
ZnPT [1μM]
g
HSP70
HO-1
α-actin
time [h]
PJ-34
ZnPT
h
control
ZnPT [500 nM]
PARP-1wt
PARP-1-/-
93.5 ± 0.9
30.6 ± 9.5
90.9 ± 1.8
78.8 ± 6.3
PI
annexinV-FITC
i
Ponceau
PAR
170
130
95
72
55
43
34
26
Mw
[kDa]
0 5 15 30 60
ZnPT [5 μM]
time [min]

◀ **Fig. 4** PARP-dependent ATP depletion in ZnPT-treated human skin keratinocytes and mouse embryonal fibroblasts. **a** Time course of cellular ATP depletion in HEKs exposed to ZnPT in the absence or presence of PARP inhibitors (3-ABA, 4 mM; PJ-34, 0.5 μM; added 1 h before ZnPT). **b** Cellular ATP depletion in HEKs exposed to ZnPT (1 μM, 6 h) in the absence or presence of DTPA (60 μM; added 1 h before ZnPT). **c** Cellular glutathione levels in HEKs exposed to a dose range of ZnPT (100–1,000 nM, 6 h). Changes in cellular glutathione were not significant (*n.s.*). **d** Time course of cellular ATP depletion in PARP$^{-/-}$ versus wild-type MEFs exposed to ZnPT (mean ± SD, n=3). **e** Immunoblot detection of PARP-1 protein in PARP$^{-/-}$ versus wild-type MEFs. **f** Western blot analysis of ZnPT-induced HSP70 upregulation in PARP$^{-/-}$ versus wild-type MEFs as a function of exposure time. **g** Western blot analysis of ZnPT (500 nM)-induced HSP70 and HO-1 upregulation in HEKs as a function of exposure time and PJ-34 pretreatment (0.5 μM). **h** Induction of cell death in PARP$^{-/-}$ versus wild-type MEFs upon exposure to ZnPT (24 h) as assessed in Fig. 1b–d. The *numbers* indicate viable cells (AV$^-$, PI$^-$, *lower left quadrant*) in percent of total gated cells (mean ± SD, three independent experiments). Flow cytometric panels depict one representative experiment. **i** Formation of poly(ADP-ribose) polymer (*PAR*)-modified cellular proteins as detected by immunoblotting of cellular extracts obtained from HEKs exposed to ZnPT (5 μM) as a function of exposure time. *Left panel* Ponceau-stained nitrocellulose membrane confirming equal protein loading; *right panel* PAR immunoblot

Cellular glutathione levels, an important indicator of cellular oxidative stress, did not change in response to ZnPT treatment (Fig. 4c; 6-h exposure; total glutathione level of untreated controls=74.4±9.6 nmol/mg protein, n=3), suggesting that oxidative stress was not involved in early induction of cytotoxicity and energy crisis in response to ZnPT treatment. Indeed, flow cytometric analysis using DCFH-DA as a peroxide probe and dihydroethidium as a superoxide probe, a standard methodology for the assessment of cellular oxidative stress as discussed elsewhere (Wondrak 2007b; Cabello et al. 2009a), did not reveal changes in cellular ROS levels in response to ZnPT treatment over the course of a 24-h observational range (data not shown).

In contrast, ZnPT-induced ATP depletion was prevented by co-administration of 3-aminobenzamide (3-ABA), an established inhibitor of PARP, an enzyme involved in induction of energy crisis in response to genotoxic stress (Fig. 4a; Burkle 2001; Pogrebniak et al. 2003; Zong et al. 2004; Kehe et al. 2008). This result was independently confirmed using the more potent and selective PARP inhibitor PJ-34 (Fig. 4a; Ethier et al. 2007). Moreover, using PARP-1 knockout (PARP-1$^{-/-}$) and wild-type (PARP-1^{wt}) mouse embryonic fibroblasts (Wang et al. 1995), it was observed that ATP depletion by ZnPT treatment was blocked in PARP-1$^{-/-}$ cells, providing compelling genetic evidence in support of PARP-1 involvement in ZnPT induced ATP depletion (Fig. 4d, e). In contrast, ZnPT-induced upregulation of heat shock protein expression occurred independent of PARP expression in MEFs (Fig. 4f); equally, HSP70 and HO-1 upregulation in HEKs exposed to ZnPT occurred irrespective of pharmacological PARP antagonism (PJ-34; Fig. 4g). These data suggest that PARP activation is not required for the induction of heat shock protein expression in response to ZnPT. Moreover, PARP-1$^{-/-}$ cells, but not PARP-1^{wt} cells, displayed pronounced resistance to ZnPT-induced cytotoxicity, maintaining viability during extended exposure (Fig. 4h). Independent confirmation of ZnPT-induced activation of PARP activity was obtained by immunodetection of PAR-modified cellular proteins (Fig. 4i). Indeed, massive PAR formation was observed in HEKs within 15-min exposure to ZnPT (5 μM) and disappeared within an hour indicating rapid polymer turnover.

Taken together, these data provide pharmacological and genetic evidence in support of PARP-1-dependent ATP depletion as a crucial mechanism underlying ZnPT cytotoxicity in HEKs.

ZnPT treatment rapidly impairs genomic integrity in human epidermal keratinocytes Pronounced induction of cellular stress gene expression (Figs. 1 and 2) and cytotoxicity observed at low concentrations of ZnPT (Fig. 3) combined with rapid ATP depletion that was prevented by PARP antagonism (Fig. 4) led us to examine the possibility that ZnPT induces DNA damage in HEKs. Using alkaline single-cell gel electrophoresis (comet assay) as a sensitive genotoxicity assay (Singh et al. 1988; Tice et al. 2000; Roberts et al. 2003), the integrity of cellular DNA was examined in HEKs treated with ZnPT (100 and 500 nM, 1 up to 12 h of exposure time). As positive controls, cells were exposed to H_2O_2, an established genotoxic agent. Exposure to submicromolar concentrations of ZnPT significantly impaired HEK genomic integrity within 1 h of exposure time as evident from formation of nuclear comets (Fig. 5a, b), whereas no comet formation was observed as a result of exposure to $ZnSO_4$ (1 μM; data not shown). ZnPT treatment (500 nM) induced comets with average tail moments that were increased approximately 3-fold over untreated controls within 1 h of exposure and exceeded control levels approximately 5-fold within 12 h of exposure (Fig. 5a).

It is important to note that loss of genomic integrity occurred in cells without compromised viability maintained over 6 h of continuous exposure as demonstrated earlier (ZnPT 500 nM, Fig. 3c). Remarkably, significant comet formation was even observed at very low ZnPT concentrations (100 nM, Fig. 5a) that do not impair viability at any time point of observation (Fig. 3b). Moreover, ZnPT induction of comets occurred irrespective of PARP status as suggested by equal comet formation in response to ZnPT observed in PARP-1$^{-/-}$ versus wild-type MEFs (data not shown). This suggests that ZnPT-induced early DNA

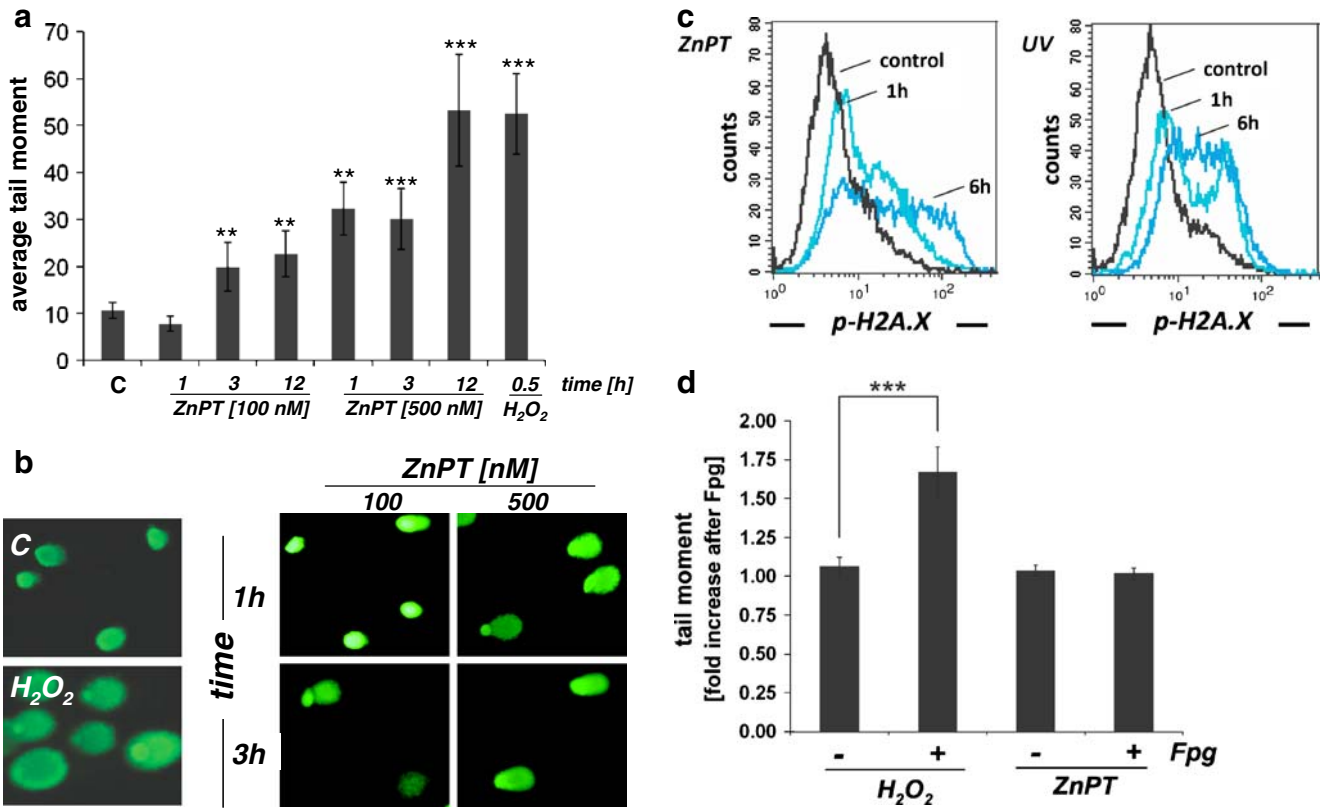

Fig. 5 Impairment of genomic integrity in ZnPT-treated human skin keratinocytes. **a** Average comet tail moments. HEKs were exposed to ZnPT (100–500 nM; 1 to 12 h), and DNA damage was detected using the alkaline comet assay. As a positive control, cells were exposed to H_2O_2 (100 μM, 30 min). **b** Representative comets as visualized by fluorescence microscopy. *C* untreated control, *H_2O_2* positive control; *right panels* ZnPT. **c** Induction of g-H2A.X in ZnPT-treated HEKs (1 μM, 1 and 6 h of exposure, *left panel*). As a positive control, g-H2A.X was detected in UVB-treated (240 mJ/cm^2) cells (1 and 6 h after UV, *right panel*). **d** Assessment of oxidative DNA damage using the Fpg-endonuclease modified comet assay. Cells were exposed to ZnPT (500 nM; 3 h) or H_2O_2 (100 μM; 20 min). Fold increase in mean tail moment of nuclei after incubation in buffer plus Fpg versus buffer only was calculated as specified in "Materials and methods"

damage does not result from a general loss of cell integrity or energy crisis and that PARP-mediated ATP depletion in ZnPT-exposed HEKs (Fig. 4) is a consequence of impaired DNA integrity, a mechanistic link between genotoxic insult, PARP activation, and energy depletion established for many genotoxic agents (Burkle 2001; Pogrebniak et al. 2003; Zong et al. 2004; Kehe et al. 2008).

In order to obtain independent experimental evidence in support of ZnPT-induced DNA damage, we used flow cytometric detection of the nuclear phosphorylated histone variant H2A.X (γ-H2A.X, Ser 139), a sensitive marker of DNA double-strand breaks and UVB-induced nucleotide excision repair (Fig. 5c; Hanasoge and Ljungman 2007; Kinner et al. 2008). Massive induction of γ-H2A.X was observed in response to UVB exposure serving as a positive control. Importantly, significant upregulation of γ-H2A.X was observed in HEKs exposed to ZnPT (1 μM, 6 h) and was detectable at time points as early as 1 h, suggesting a ZnPT-induced early impairment of genomic integrity in HEKs.

DNA comets formed from DNA unwinding under alkaline conditions are indicative of impaired genomic integrity resulting from single- or double-strand breaks, AP-site formation, or nucleotide excision repair (Tice et al. 2000). Protection from ZnPT-induced cytotoxicity by the thiol antioxidant NAC (Fig. 3d) therefore led us to examine the possibility that ZnPT-associated comets in HEKs originate from oxidative DNA damage. To this end, we performed comet analysis under conditions that detect oxidative base damage (Tice et al. 2000), assessing Fpg-induced strand cleavage at oxidized DNA purine bases (Fig. 5d). Indeed, in H_2O_2-treated control cells, mean comet tail moment was increased after Fpg-endonuclease treatment by approximately 70% consistent with oxidative generation of Fpg-sensitive sites. However, mean comet tail moment remained unchanged in ZnPT-exposed cells irrespective of Fpg treatment, providing experimental evidence against introduction of oxidative DNA damage by ZnPT exposure.

Taken together, these data disqualify the possibility that ZnPT-induced DNA damage results from the induction of cellular oxidative stress. Therefore, the absence of ZnPT-induced ROS formation (data not shown), glutathione

depletion (Fig. 4c), and oxidative DNA damage (Fig. 5d) combined with the lack of protection observed with all antioxidant treatments except NAC (Fig. 3d) suggest that NAC antagonism of ZnPT cytotoxicity may rather originate from thiol-based chemical interference with ZnPT complex integrity rather than antioxidant activity (Barnett et al. 1977).

Based on these data, it was concluded that ZnPT-induced loss of genomic integrity in HEKs (I) occurs rapidly upon exposure to nanomolar concentrations before general impairment of cell viability and (II) occurs upstream of massive ATP depletion through PARP activation that does not originate from oxidative DNA damage.

ZnPT impairs genomic integrity of human epidermal melanocytes with induction of energy crisis and heat shock protein upregulation In an attempt to further explore the effects of ZnPT exposure on other human epidermal skin cells, we examined primary human epidermal melanocytes (HEMs) as potential target cells. Indeed, antiproliferative effects on melanocytes were observed at doses even lower than those active against HEKs; almost complete inhibition of proliferation occurred at a threshold concentration of 100 nM ZnPT (Fig. 6a). However, no induction of cell death was observed at this concentration, and loss of viability was only observed upon exposure to much higher concentrations (2 μM; 24 h; data not shown). As observed with HEKs (Fig. 2b, c), upregulation of HSP70 protein levels was detected in response to submicromolar concentrations ZnPT (Fig. 6b). Moreover, massive ATP depletion by ZnPT occurred at early timepoints (1 h exposure) in HEMs (Fig. 6c). This effect was again significantly antagonized by pharmacological PARP inhibition (3-ABA), a situation closely resembling PARP-dependent ATP depletion in response to ZnPT-induced genotoxic stress in HEKs (Fig. 4a). Importantly, comet analysis demonstrated that ZnPT treatment rapidly impaired genomic integrity of HEMs, with approximately 20-fold elevation of mean tail moment observed within 1 h of exposure (ZnPT 500 nM; Fig. 6d).

Taken together, these data demonstrate that ZnPT-induced inhibition of proliferation, impairment of genomic integrity, and rapid ATP depletion not only can be observed in HEKs but also occurs in HEMs as another relevant cellular target in the human epidermis.

Discussion

ZnPT is an important FDA-approved microbicidal OTC drug, and annual production of ZnPT for FDA-regulated applications in skin products, including creams, sprays, and shampoos, now exceeds 450,000 kg in the USA alone (Pierard-Franchimont et al. 2002; Bailey et al. 2003; Smegal et al. 2004; Guthery et al. 2005).

Our data obtained in a primary skin cell culture system document for the first time the exquisite vulnerability of primary keratinocytes and melanocytes to nanomolar concentrations of ZnPT that rapidly induce a massive heat shock response and loss of genomic integrity.

ZnPT-dependent upregulation of the cellular heat shock response observed here in cultured human skin cells is consistent with earlier findings that demonstrated the ability of zinc ions to induce the heat shock response involved in cytoprotective and cytotoxic activities of this micronutrient in mammalian cells (Hatayama et al. 1993; Lee et al. 2000; Unoshima et al. 2001). Upregulation of the cellular heat shock response in human epidermal cells occurred at submicromolar doses of ZnPT that also induced inhibition of cell proliferation and cell death (Figs. 3 and 6), therefore excluding feasibility of dissociating cytoprotective from cytotoxic effects of ZnPT as originally intended at the beginning of this study.

In addition to induction of heat shock response gene expression in HEKs, we observed that ZnPT treatment caused rapid depletion of cellular ATP levels (Fig. 4a). Both pharmacological inhibition of PARP-1 (Fig. 4a) and genetic elimination using engineered PARP-$1^{-/-}$ MEFs (Fig. 4d, e) antagonized ZnPT-induced early depletion of cellular ATP levels. These data provide compelling evidence for activation of PARP in response to ZnPT treatment, further confirmed by detection of PAR-modified cellular proteins within minutes of exposure to ZnPT (Fig. 4i).

It is well established that PARP activation occurs in response to genotoxic stress, leading to rapid cellular NAD and ATP depletion (Burkle 2001; Pogrebniak et al. 2003; Zong et al. 2004; Meyer-Ficca et al. 2005; Ethier et al. 2007; Kehe et al. 2008). Direct evidence for ZnPT-induced DNA damage was obtained by comet analysis (Fig. 5a) and phosphorylation of histone H2A.X at serine 139 (γ-H2A.X; Fig. 5c). Similar results were obtained in human primary melanocytes based on comet analysis (Fig. 6d) and determination of PARP-dependent ATP depletion (Fig. 6c).

The molecular mechanism of skin cell DNA damage caused by this widely used topical drug is currently unknown, and multiple mechanisms may underlie the detrimental effect of ZnPT on skin cell genomic integrity. For example, it has been shown earlier that disruption of intracellular zinc homeostasis is an important activator of endonucleases including DNase gamma (Shiokawa and Tanuma 1998). Moreover, exposure to high levels of zinc ions can be associated with formation of reactive oxygen species that would provide another mechanistic basis for the genotoxic effects of ZnPT (Cabreiro et al. 2009). However, consistent with the absence of ZnPT-induced

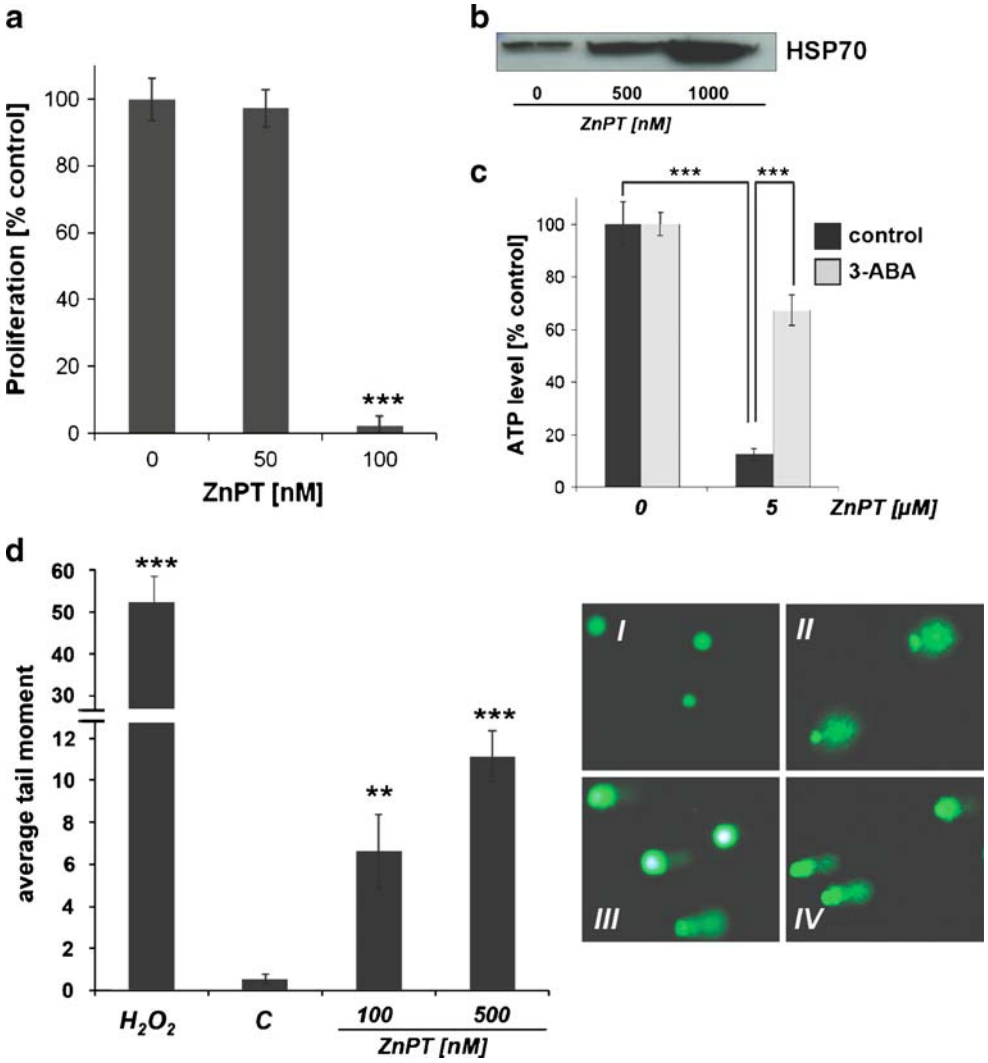

Fig. 6 ZnPT-induced impairment of proliferation, genomic integrity, and ATP homeostasis with upregulated HSP70 expression in human skin melanocytes. **a** Dose response relationship of ZnPT-induced inhibition of cell proliferation. After 72 h of exposure to increasing concentrations of ZnPT, proliferation was determined as specified in Fig. 3a. **b** Dose response of ZnPT-induced HSP70 protein upregulation by immunoblot analysis (24 h of exposure). **c** Cellular ATP depletion induced by ZnPT (1 h) in the absence or presence of 3-ABA (4 mM, added 1 h before ZnPT). **d** Average comet tail moment induced by ZnPT (1 h exposure) and H_2O_2 (100 µM, 30 min exposure) performed as detailed in Fig. 5a. *I–IV* depict representative comets as visualized by fluorescence microscopy: *I* untreated control, *II* H_2O_2, *III* ZnPT (100 nM), *IV* ZnPT (500 nM)

oxidative cellular stress as assessed by fluorescent redox probes and determination of cellular glutathione levels (Fig. 4c), our experiments that detect Fpg-endonuclease-sensitive oxidative lesions gave no indication for the generation of oxidative DNA damage as a consequence of exposure to nanomolar concentrations of ZnPT (Fig. 5d).

Earlier experiments demonstrate that exposure of mammalian cells to various zinc salts (e.g., $ZnSO_4$, $ZnCl_2$, and Zn acetate) is well tolerated at concentrations up to 200 µM without reduction of viability (Hatayama et al. 1993; Jourdan et al. 2002; Cortese et al. 2008). However, potentiation of zinc effects and induction of cytotoxicity by zinc-specific ionophores, including pyrithione, has been observed earlier (Kim et al. 1999; Magda et al. 2008), and cytotoxic effects of ZnPT on cultured mammalian cells of non-cutaneous origin have been associated with disruption of intracellular zinc homeostasis and activation of signaling cascades including the ras/ERK pathway (Mann and Fraker 2005; Klein et al. 2006). In our own experiments using HEKs, ZnPT induction of cell death occurred without involvement of caspases and was characterized by early PARP activation and rapid cellular ATP depletion, a molecular pathway reminiscent of many genotoxic agents known to induce caspase-independent cell death orchestrated by PARP activation (Zong et al. 2004; Ethier et al. 2007; Cohausz et al. 2008).

The FDA code of federal regulations (21CFR § 358.710) specifies the use of ZnPT as an active OTC ingredient for the control of dandruff and seborrheic dermatitis. It is important to note that epidermal deposition and retention of ZnPT following topical application has been demonstrated in human skin (Rutherford and Black 1969; Leyden et al. 1979). Skin permeation of radiolabeled ZnPT leading to urinary excretion of up to 0.2% of topically applied starting material has been documented in rhesus monkeys (Gibson and Calvin 1978), and ZnPT absorption was increased strongly when the integrity of the stratum corneum was disrupted by abrasion or repeated exposure to concentrated

surfactant solutions. Toxicological concerns have been raised earlier based on cytotoxicity and genotoxicity observed in mouse lymphoma cells and embryotoxicity observed in fish (Goka 1999; Moller et al. 2002), and no published experimental study has examined the potential cyto- and genotoxic activity of ZnPT on cultured primary human skin cells (Smegal et al. 2004).

Taken together, earlier studies raise the possibility that topically applied ZnPT may indeed penetrate deep enough into the living human epidermis to impair human skin cell genomic integrity as observed here in cultured cells. Moreover, the known solubility of ZnPT in skin sebum and its retention in hair follicles observed previously suggest that topically applied ZnPT may also reach crucial stem cell populations in human skin hair follicles (Guthery et al. 2005). However, our cell culture system does not adequately represent human epidermal skin with intact barrier function that may limit exposure of living epidermal cells to the cytotoxic concentrations established in our experiments.

The important question of whether topical application of ZnPT coformulated with or without detergents can target and compromise keratinocytes and melanocytes in intact human skin and hair follicles is currently being addressed in our laboratory using relevant models with intact barrier function including terminally differentiated epidermal skin reconstructs and intact human skin ex vivo (Bause et al. 2009).

Acknowledgments Supported in part by grants from the National Institutes of Health (Award Number R01CA122484 from the National Cancer Institute, ES007091, ES06694, Arizona Cancer Center Support Grant CA023074), NSF (DGE-0114420 to CMC), and the Arizona Science Foundation (to SL). The content is solely the responsibility of the author and does not necessarily represent the official views of the National Cancer Institute or the National Institutes of Health.

References

Bailey P, Arrowsmith C, Darling K, Dexter J, Eklund J, Lane A, Little C, Murray B, Scott A, Williams A, Wilson D (2003) A double-blind randomized vehicle-controlled clinical trial investigating the effect of ZnPTO dose on the scalp vs. antidandruff efficacy and antimycotic activity. Int J Cosmet Sci 25:183–188

Barnett BL, Kretschmar HC, Hartman FA (1977) Structural characterization of bis(N-oxopyridine-2-thionato)zinc(II). Inorg Chem 16:1834–1838

Baudouin C, Charveron M, Tarroux R, Gall Y (2002) Environmental pollutants and skin cancer. Cell Biol Toxicol 18:341–348

Bause AS, Lamore SD, Wondrak GT (2009) More than skin deep: the human skin tissue equivalent as an advanced drug discovery tool. Frontiers Drug Design Discov 4:135–161

Brandrup F, Menne T (1985) Zinc pyrithione (zinc omadine) allergy. Contact Dermatitis 12:50

Burkle A (2001) Poly(APD-ribosyl)ation, a DNA damage-driven protein modification and regulator of genomic instability. Cancer Lett 163:1–5

Cabello CM, Bair WB 3rd, Lamore SD, Ley S, Bause AS, Azimian S, Wondrak GT (2009a) The cinnamon-derived Michael acceptor cinnamic aldehyde impairs melanoma cell proliferation, invasiveness, and tumor growth. Free Radic Biol Med 46:220–231

Cabello CM, Bair WB 3rd, Ley S, Lamore SD, Azimian S, Wondrak GT (2009b) The experimental chemotherapeutic N(6)-furfuryladenosine (kinetin-riboside) induces rapid ATP depletion, genotoxic stress, and CDKN1A (p21) upregulation in human cancer cell lines. Biochem Pharmacol 77:1125–1138

Cabreiro F, Picot CR, Perichon M, Friguet B, Petropoulos I (2009) Overexpression of methionine sulfoxide reductases A and B2 protects MOLT-4 cells against zinc-induced oxidative stress. Antioxid Redox Signal 11:215–225

Chuong CM, Nickoloff BJ, Elias PM, Goldsmith LA, Macher E, Maderson PA, Sundberg JP, Tagami H, Plonka PM, Thestrup-Pederson K, Bernard BA, Schroder JM, Dotto P, Chang CM, Williams ML, Feingold KR, King LE, Kligman AM, Rees JL, Christophers E (2002) What is the 'true' function of skin? Exp Dermatol 11:159–187

Cohausz O, Blenn C, Malanga M, Althaus FR (2008) The roles of poly(ADP-ribose)-metabolizing enzymes in alkylation-induced cell death. Cell Mol Life Sci 65:644–655

Cortese MM, Suschek CV, Wetzel W, Kroncke KD, Kolb-Bachofen V (2008) Zinc protects endothelial cells from hydrogen peroxide via Nrf2-dependent stimulation of glutathione biosynthesis. Free Radic Biol Med 44:2002–2012

Dinkova-Kostova AT, Jenkins SN, Fahey JW, Ye L, Wehage SL, Liby KT, Stephenson KK, Wade KL, Talalay P (2006) Protection against UV-light-induced skin carcinogenesis in SKH-1 high-risk mice by sulforaphane-containing broccoli sprout extracts. Cancer Lett 240:243–252

Ethier C, Labelle Y, Poirier GG (2007) PARP-1-induced cell death through inhibition of the MEK/ERK pathway in MNNG-treated HeLa cells. Apoptosis 12:2037–2049

Gibson WB, Calvin G (1978) Percutaneous absorption of zinc pyridinethione in monkeys. Toxicol Appl Pharmacol 43:425–437

Goka K (1999) Embryotoxicity of zinc pyrithione, an antidandruff chemical, in fish. Environ Res 81:81–83

Guthery E, Seal LA, Anderson EL (2005) Zinc pyrithione in alcohol-based products for skin antisepsis: persistence of antimicrobial effects. Am J Infect Control 33:15–22

Halliday GM (2005) Activation of molecular adaptation to sunlight—a new approach to photoprotection. J Invest Dermatol 125:xviii–xix

Hanasoge S, Ljungman M (2007) H2AX phosphorylation after UV irradiation is triggered by DNA repair intermediates and is mediated by the ATR kinase. Carcinogenesis 28:2298–2304

Hatayama T, Asai Y, Wakatsuki T, Kitamura T, Imahara H (1993) Regulation of hsp70 synthesis induced by cupric sulfate and zinc sulfate in thermotolerant HeLa cells. J Biochem 114:592–597

Howes D, Black JG (1975) Comparative percutaneous absorption of pyrithiones. Toxicology 5:209–220

Jonak C, Klosner G, Trautinger F (2009) Significance of heat shock proteins in the skin upon UV exposure. Front Biosci 14:4758–4768

Jourdan E, Emonet-Piccardi N, Didier C, Beani JC, Favier A, Richard MJ (2002) Effects of cadmium and zinc on solar-simulated light-irradiated cells: potential role of zinc-metallothionein in zinc-induced genoprotection. Arch Biochem Biophys 405:170–177

Kehe K, Raithel K, Kreppel H, Jochum M, Worek F, Thiermann H (2008) Inhibition of poly(ADP-ribose) polymerase (PARP) influences the mode of sulfur mustard (SM)-induced cell death in HaCaT cells. Arch Toxicol 82:461–470

Kim CH, Kim JH, Moon SJ, Chung KC, Hsu CY, Seo JT, Ahn YS (1999) Pyrithione, a zinc ionophore, inhibits NF-kappaB activation. Biochem Biophys Res Commun 259:505–509

Kinner A, Wu W, Staudt C, Iliakis G (2008) Gamma-H2AX in recognition and signaling of DNA double-strand breaks in the context of chromatin. Nucleic Acids Res 36:5678–5694

Klein C, Creach K, Irintcheva V, Hughes KJ, Blackwell PL, Corbett JA, Baldassare JJ (2006) Zinc induces ERK-dependent cell death through a specific Ras isoform. Apoptosis 11:1933–1944

Kullavanijaya P, Lim HW (2005) Photoprotection. J Am Acad Dermatol 52:937–958 quiz 959-962

Lee JY, Park J, Kim YH, Kim DH, Kim CG, Koh JY (2000) Induction by synaptic zinc of heat shock protein-70 in hippocampus after kainate seizures. Exp Neurol 161:433–441

Leyden JJ, Stewart R, Kligman AM (1979) Updated in vivo methods for evaluating topical antimicrobial agents on human skin. J Invest Dermatol 72:165–170

Magda D, Lecane P, Wang Z, Hu W, Thiemann P, Ma X, Dranchak PK, Wang X, Lynch V, Wei W, Csokai V, Hacia JG, Sessler JL (2008) Synthesis and anticancer properties of water-soluble zinc ionophores. Cancer Res 68:5318–5325

Mann JJ, Fraker PJ (2005) Zinc pyrithione induces apoptosis and increases expression of Bim. Apoptosis 10:369–379

Merwald H, Kokesch C, Klosner G, Matsui M, Trautinger F (2006) Induction of the 72-kilodalton heat shock protein and protection from ultraviolet B-induced cell death in human keratinocytes by repetitive exposure to heat shock or 15-deoxy-delta(12, 14)-prostaglandin J2. Cell Stress Chaperones 11:81–88

Meyer-Ficca ML, Meyer RG, Jacobson EL, Jacobson MK (2005) Poly (ADP-ribose) polymerases: managing genome stability. Int J Biochem Cell Biol 37:920–926

Moller M, Adam W, Saha-Moller CR, Stopper H (2002) Studies on cytotoxic and genotoxic effects of N-hydroxypyridine-2-thione (Omadine) in L5178Y mouse lymphoma cells. Toxicol Lett 136:77–84

Noonan EJ, Place RF, Giardina C, Hightower LE (2007) Hsp70B′ regulation and function. Cell Stress Chaperones 12:219–229

Okamoto K, Ito T, Hasegawa A (1967) Percutaneous absorption of zin bis-(2-pyridylthio)-1, 1′-dioxide and residual amounts left on the surface of the skin. Eisei Kagaku 13:323–329

Pierard-Franchimont C, Goffin V, Decroix J, Pierard GE (2002) A multicenter randomized trial of ketoconazole 2% and zinc pyrithione 1% shampoos in severe dandruff and seborrheic dermatitis. Skin Pharmacol Appl Skin Physiol 15:434–441

Pogrebniak A, Schemainda I, Pelka-Fleischer R, Nussler V, Hasmann M (2003) Poly ADP-ribose polymerase (PARP) inhibitors transiently protect leukemia cells from alkylating agent induced cell death by three different effects. Eur J Med Res 8:438–450

Roberts MJ, Wondrak GT, Cervantes-Laurean D, Jacobson MK, Jacobson EL (2003) DNA damage by carbonyl stress in human skin cells. Mutat Res 522:45–56

Rutherford T, Black JG (1969) The use of autoradiography to study the localization of germicides in skin. Br J Dermatol 81:75–86

Shiokawa D, Tanuma S (1998) Molecular cloning and expression of a cDNA encoding an apoptotic endonuclease DNase gamma. Biochem J 332(Pt 3):713–720

Singh NP, McCoy MT, Tice RR, Schneider EL (1988) A simple technique for quantitation of low levels of DNA damage in individual cells. Exp Cell Res 175:184–191

Skoulis NP, Barbee SJ, Jacobson-Kram D, Putman DL, San RH (1993) Evaluation of the genotoxic potential of zinc pyrithione in the Salmonella mutagenicity (Ames) assay, CHO/HGPRT gene mutation assay and mouse micronucleus assay. J Appl Toxicol 13:283–289

Smegal D, McMahon TF, Aviado D, Montague K, Shamim N, Mostaghimi S [EPA A.D.] (2004) Zinc pyrithione (zinc omadine): AD Risk Assessment for the Reregistration Eligibility Decision (RED) Document; Chemical No. 088002. Case No. 2480. DP Barcode: D308704. ID: EPA-HQ-OPP-2004-0147-0023; www.regulations.gov. 1–51

Snyder FH, Buehler EV, Winek CL (1965) Safety evaluation of zinc 2-pyridinethiol 1-oxide in a shampoo formulation. Toxicol Appl Pharmacol 7:425–437

Tice RR, Agurell E, Anderson D, Burlinson B, Hartmann A, Kobayashi H, Miyamae Y, Rojas E, Ryu JC, Sasaki YF (2000) Single cell gel/comet assay: guidelines for in vitro and in vivo genetic toxicology testing. Environ Mol Mutagen 35:206–221

Unoshima M, Nishizono A, Takita-Sonoda Y, Iwasaka H, Noguchi T (2001) Effects of zinc acetate on splenocytes of endotoxemic mice: enhanced immune response, reduced apoptosis, and increased expression of heat shock protein 70. J Lab Clin Med 137:28–37

Wang ZQ, Auer B, Stingl L, Berghammer H, Haidacher D, Schweiger M, Wagner EF (1995) Mice lacking ADPRT and poly(ADP-ribosyl)ation develop normally but are susceptible to skin disease. Genes Dev 9:509–520

Wondrak GT (2007a) Let the sun shine in: mechanisms and potential for therapeutics in skin photodamage. Curr Opin Investig Drugs 8:390–400

Wondrak GT (2007b) NQO1-activated phenothiazinium redox cyclers for the targeted bioreductive induction of cancer cell apoptosis. Free Radic Biol Med 43:178–190

Wondrak GT, Roberts MJ, Cervantes-Laurean D, Jacobson MK, Jacobson EL (2003) Proteins of the extracellular matrix are sensitizers of photo-oxidative stress in human skin cells. J Invest Dermatol 121:578–586

Wondrak GT, Jacobson MK, Jacobson EL (2006) Endogenous UVA-photosensitizers: mediators of skin photodamage and novel targets for skin photoprotection. Photochem Photobiol Sci 5:215–237

Wondrak GT, Cabello CM, Villeneuve NF, Zhang S, Ley S, Li Y, Sun Z, Zhang DD (2008) Cinnamoyl-based Nrf2-activators targeting human skin cell photo-oxidative stress. Free Radic Biol Med 45:385–395

Zong WX, Ditsworth D, Bauer DE, Wang ZQ, Thompson CB (2004) Alkylating DNA damage stimulates a regulated form of necrotic cell death. Genes Dev 18:1272–1282